NEOPLASIA
www.neoplasia.com
Volume 23 Number xxx Month 2021 pp. 473–487

Original research

SalvGlandDx – a comprehensive salivary gland neoplasm specific next generation sequencing panel to facilitate diagnosis and identify therapeutic targets ☆, ☆☆

Sandra N. Freiberger [a,m]; Muriel Brada [a,m]; Christine Fritz [a,m]; Sylvia Höller [a,m]; Alexander Vogetseder [b]; Milo Horcic [c]; Michel Bihl [d]; Michal Michal [e,f]; Martin Lanzer [g,m]; Martin Wartenberg [h]; Urs Borner [i]; Peter K. Bode [a,m]; Martina A. Broglie [j,m]; Tamara Rordorf [k,m]; Grégoire B. Morand [j,l,m]; Niels J. Rupp [a,m,*]

[a] Department of Pathology and Molecular Pathology, University Hospital Zurich, Zurich, Switzerland
[b] Department of Pathology, Cantonal Hospital of Lucerne, Lucerne, Switzerland
[c] Institute for Histological and Cytological Diagnostics AG, Aarau, Switzerland
[d] Department of Pathology and Medical Genetics, University Hospital Basel, Basel, Switzerland
[e] Sikl's Department of Pathology, Medical Faculty in Pilsen, Charles University in Prague, Pilsen, Czech Republic
[f] Bioptical Laboratory, Pilsen, Czech Republic
[g] Department of Oral and Maxillofacial Surgery, University Hospital Zurich, Zurich, Switzerland
[h] Institute of Pathology, University of Bern, Bern, Switzerland
[i] Department of Otorhinolaryngology, Head and Neck Surgery, Inselspital, Bern University Hospital and University of Bern, Bern, Switzerland
[j] Department of Otorhinolaryngology, Head and Neck Surgery, University Hospital Zurich, Zurich, Switzerland
[k] Department of Medical Oncology, University Hospital Zurich, Zurich, Switzerland
[l] Department of Otolaryngology-Head and Neck Surgery, Sir Mortimer B. Davis- Jewish General Hospital, McGill University, Montreal, Quebec, Canada
[m] University of Zurich, Zurich, Switzerland

Abstract

Diagnosis of salivary gland neoplasms is often challenging due to their high morphological diversity and overlaps. Several recurrent molecular alterations have been described recently, which can serve as powerful diagnostic tools and potential therapeutic targets (e.g. *NTRK* or *RET* fusions). However, current sequential molecular testing can be expensive and time consuming. In order to facilitate the diagnosis of salivary gland neoplasms, we designed an all-in-one RNA-based next generation sequencing panel suitable for the detection of mutations, fusions and gene expression levels (including *NR4A3*) of 27 genes involved in salivary gland neoplasms. Here we present the validation of the "SalvGlandDx" panel on FFPE histological specimen including fine needle aspiration (FNA) cell block material, against the standard methods currently used at our institution. In a second part we describe selected unique cases in which the SalvGlandDx panel allowed proper diagnosis and new insights into special molecular characteristics of selected salivary gland tumors. We characterize a unique salivary gland adenocarcinoma harboring a *ZCCHC7-NTRK2* fusion, a highly uncommon spindle cell and pseudoangiomatoid adenoid-cystic carcinoma with *MYBL1-NFIB* fusion, and a purely oncocytic mucoepidermoid carcinoma, whereas diagnosis could be made by detection of a *CRTC3-MAML2* rearrangement on the cell block specimen of the

* Corresponding author: Niels J. Rupp, MD, Department of Pathology and Molecular Pathology, University Hospital Zurich, Schmelzbergstrasse 12, 8091 Zurich, Switzerland, Tel. +41 44 255 50 91, Fax. +41 44 255 44 40
E-mail address: niels.rupp@usz.ch (N.J. Rupp).
☆ ☆Funding: MH received institutional funding from Roche outside the submitted work. NJR discloses an advisory board function and receipt of honoraria from F. Hoffmann-La Roche AG. The "SalvGlandDx" panel has been developed by a grant from the Iten-Kohaut-Foundation / University Hospital Zurich Foundation to NJR.
☆☆ Conflict of interest: All other authors declare that they have no conflict of interest.

Received 31 January 2021; received in revised form 21 March 2021; accepted 22 March 2021

https://doi.org/10.1016/j.neo.2021.03.008

FNA. Further, a rare case of a *SS18-ZBTB7A* rearranged low-grade adenocarcinoma previously described as potential spectrum of microsecretory adenocarcinoma, is reported. In addition, features of six cases within the spectrum of polymorphous adenocarcinoma / cribriform adenocarcinoma of salivary gland including *PRKD1* p.E710D mutations and novel fusions involving *PRKAR2A-PRKD1, SNX9-PRKD1* and *ATL2-PRKD3,* are described.

Neoplasia (2021) 23, 473–487

Keywords: Salivary gland neoplasm, Biopsy, FNA, Molecular, Comprehensive, Testing

Introduction

Salivary gland neoplasms often show a broad morphological spectrum including a variety of overlapping morphological patterns between different entities [1]. The diagnosis of these neoplasms can therefore pose significant difficulties. Especially on fine needle aspiration (FNA) or small biopsies, the differentiation between benign and low-grade malignant tumors can sometimes be impossible based on morphology alone [1, 2]. In recent years, the knowledge about genomic landscapes of salivary gland neoplasms has significantly increased. Thereby, the distinct molecular aberrations are often highly specific to certain entities and can be exploited for diagnostic purposes [3]. The typical molecular aberrations encompass mutations, such as recurrent activating *HRAS* and/or *PIK3CA* mutations in epithelial-myoepithelial carcinoma [4]. Furthermore, increased expression levels of *NR4A3* due to enhancer hijacking have been described recently as a hallmark of acinic cell carcinoma [5]. In addition, certain aberrations, such as *NTRK3* fusions, which are highly recurrent in (mammary analogue) secretory carcinoma provide both a diagnostic [6] and therapeutic alteration for novel targeted inhibitors [7]. To further increase the diagnostic accuracy and facilitate diagnosis of salivary gland neoplasms, we here present a custom-designed comprehensive next generation RNA sequencing panel. This approach covers most of the common molecular alterations of salivary gland neoplasms in one test and can be reliably performed on FFPE tissue including biopsy or cell block specimen of FNAs. Therefore, the SalvGlandDx panel was recently implemented in our institutional diagnostic setting.

Material and methods

Panel design

The target region was designed according to the current knowledge of molecular alterations (fusions and mutations) of salivary gland including odontogenic neoplasms (Table 1) and covers known hotspot mutations and fusion genes. Furthermore, *NR4A3* was included in the panel to measure mRNA expression levels. Moreover, *NTRK1/2/3* fusions have recently gained high importance as therapeutic targets. Therefore, these genes were included as well. The assay was designed using the Archer Assay Designer software.

Nucleic acid isolation from FFPE specimen

Surplus FFPE material from surgical or cytologic specimen was used for nucleic acid isolation. The area of interest was marked by an experienced head and neck pathologist (NJR) on a representative H&E slide. Three 0.4 mm^2 punch biopsies were then taken from the region of interest of the FFPE block. For FNA cell block specimen, four cuts of ten micrometers were cut and pooled. RNA was isolated using the Maxwell 16 LEV RNA FFPE Purification Kit and DNA was isolated using the Maxwell 16 FFPE Tissue LEV DNA Purification Kit (both Promega, Madison, WI, USA) according to the manufacturer's manual. Quantification was done using the Qubit fluorometric assay (ThermoFisher Scientific, Waltham, MA, USA).

Library preparation and next generation sequencing (NGS)

Library preparation for the SalvGlandDx panel and the Archer FusionPlexSarcoma panel was performed according to the protocol of the Archer FusionPlex technology (ArcherDX, Boulder, CO, USA), using 250 ng input RNA. Libraries were sequenced with 150bp paired-end on a NextSeq550. Library preparation for the custom-extended Archer FusionPlexSarcoma panel was performed according to the manufacturer's protocol (ArcherDX, Boulder, CO, USA), using 250 ng input RNA. Libraries were sequenced on the Ion S5 system (ThermoFisher Scientific, Waltham, MA, USA).

Library preparation for the Oncomine Focus Assay and Oncomine Comprehensive Assay v3 was performed according to the manufacturer's manual (ThermoFisher Scientific, Waltham, MA, USA), using 10 ng or 20 ng of input material. Libraries were templated on Ion 540 chips using the Ion Chef Instrument and sequenced on the Ion S5 system (ThermoFisher Scientific, Waltham, MA, USA).

Fluorescence in situ hybridization (FISH)

Two μm thick sections were incubated with dual color break apart (bap) FISH probes for *EWSR1 (*Abbott Molecular Vysis LSI EWSR1 (22q12) bap, Abbott Park, IL, USA*), ETV6 (*Abbott Molecular Vysis ETV6 bap, Abbott Park, IL, USA), *MAML2* (bap Zytovision, Bremerhaven, Germany), *MYB* (bap Zytovision, Bremerhaven, Germany), *MYBL1* (bap Empire Genomics, Williamsville, NY, USA), *NTRK2* (bap Zytovision, Bremerhaven, Germany) and *SS18* (bap Abbott molecular, Abbott Park, IL, USA) according to the manufacturer's protocol. 50 non-overlapping nuclei were analyzed using a fluorescence microscope (Zeiss Axioskop) with a 100-fold magnification oil objective. Pictures with Z-stacks of 20 images with 0.5 μm step distance were performed. Positive FISH was defined as at least 15% cells with break-apart and /or split signals.

Sanger sequencing (PRKD1)

DNA was amplified using custom primers covering the *PRKD1* p.E710 hotspot. The resulting products were purified using the Qiagen MiniElute PCR Purification Kit (Qiagen, Hilden, Germany) and sequenced as described previously [51] using the following primers:

Primer *PRKD1*_F: 5′-TGGAAGGTGACAAGATGCTACA-3′

Primer *PRKD1*_R: 5′-ACTGGAATGAAATTTTGGTGATTCT-3′

Table 1

Molecular alterations in salivary gland and odontogenic neoplasms according to current literature.

Selected Molecular Aberrations Covered by SalvGlandDx Panel	Entity
Gene fusions	
*PLAG1** fusions	
CTNNB1-PLAG1	PA, CA ex PA, MECA [8, 9]
LIFR-PLAG1	PA, MECA [8, 9]
CHCHD7-PLAG1	PA, MECA [8, 9]
FGFR1-PLAG1	PA,CA ex PA, MECA [9–11]
ND4-PLAG1	MECA ex PA [10]
NFIB-PLAG1	PA [12]
TGFBR3-PLAG1	MECA, MECA ex PA [10]
*HMGA2** fusions	
HMGA2-WIF1	PA, CA ex PA [13]
HMGA2-NFIB	PA [12]
HMGA2-TMTC2	PA (metastasizing) [14]
*MYB** and *MYBL1** *fusions*	
MYB-NFIB	Adenoid-cystic carcinoma [15, 16]
MYBL1-NFIB	Adenoid-cystic carcinoma [15, 16]
*MAML2** fusions	
MAML2-CRTC1	Mucoepidermoid carcinoma [17]
MAML2-CRTC3	Mucoepidermoid carcinoma [18]
*PRKD1**-, *PRKD2**-, *PRKD3**- fusions	Polymorphous adenocarcinoma (including cribriform variant / CASG) [19–21]
ARID1A-PRKD1	PAC, cribriform variant / CASG [20]
DDX3X-PRKD1	PAC, cribriform variant / CASG [20]
PRKAR2A-PRKD1	PAC, cribriform variant / CASG, current study
SNX9-PRKD1	PAC, cribriform variant / CASG, current study
ATL2-PRKD3	PAC, classical variant, current study
*SS18** fusions	
SS18-MEF2C	Microsecretory adenocarcinoma (incl. potential spectrum) [22, 22] and current study
SS18-ZBTB7A	
*MSANTD3** fusions	
HTN3-MSANTD3	Acinic cell carcinoma [23]
*RET** fusions	
TRIM27-RET	Intraductal carcinoma [24]
NCOA4-RET	Intraductal carcinoma [24]
TRIM33-RET	Intraductal carcinoma [25]
VIM-RET	Secretory carcinoma [26]
ETV6* fusions	
ETV6-NTRK3	Secretory carcinoma [6]
ETV6-RET	Secretory carcinoma [27]
ETV6-MET	Secretory carcinoma [28]
*EWSR1** fusions	
EWSR1-ATF1	Clear cell (odontogenic) carcinoma [29]
EWSR1-CREB1	Clear cell (odontogenic) carcinoma [30]
EWSR1-CREM	Clear cell (odontogenic) carcinoma [31]
EWSR1-FLI1	Adamantinoma-like Ewing family tumor / sarcoma [32]
*NUTM1** fusions	
NUTM1-BRD4	NUT carcinoma [33]
NUTM1-BRD3	NUT carcinoma [34]
NUTM1-NSD3	NUT carcinoma [35]
*NTRK1**-, *NTRK2**-, *NTRK3** fusions	
ETV6-NTRK3	Secretory carcinoma [6]
NTRK2-ZCCHC7	Adenocarcinoma NOS, current study
Gene mutations	
AKT1 p.E17	Epithelial-myoepithelial carcinoma [4]
	Intraductal papillary mucinous neoplasm [36]
	Salivary mucinous adenocarcinoma [37]

(*continued on next page*)

Table 1 (*continued*)

Selected Molecular Aberrations Covered by SalvGlandDx Panel	Entity
CTNNB1 p.I35, p.Q28	Basal cell adenoma [38, 39]
SMO p.W535, p.L412	Ameloblastoma [40]
KRAS p.G12, p.G13, p.Q61	Adenomatoid odontogenic tumor [41], mucoepidermoid carcinoma [42]
PRKD1 p.E710	Polymorphous adenocarcinoma [19] (including cribriform variant) [43]
BRAF p.V600	Intraductal carcinoma [25], sialadenoma papilliferum [44], ameloblastoma [40]
HRAS p.G12, p.G13, p.Q61	Epithelial-myoepithelial carcinoma [4], intraductal carcinoma [45], salivary duct carcinoma [46], Sialadenoma papilliferum [47]
PIK3CA p.E542, p.E545, p.H1047	Salivary duct carcinoma [48], epithelial-myoepithelial carcinoma [4], sclerosing polycystic adenosis / adenoma [49], adenoid-cystic carcinoma (current study)
NRAS p.G12, p.G13, p.Q61	Salivary duct carcinoma [46]
Gene expression	
NR4A3 upregulation (due to enhancer hijacking)	Acinic cell carcinoma [5, 50]
*For each covered gene, also rare or novel fusion partners can be detected	

PA = Pleomorphic adenoma, CA ex PA = Carcinoma ex pleomorphic adenoma, MECA = Myoepithelial carcinoma, PAC = Polymorphous adenocarcinoma, CASG = cribriform adenocarcinoma of salivary gland

Immunohistochemistry

Immunohistochemical stainings were performed as described previously [52], using the monoclonal primary anti-NUT antibody (clone C52B1, 1:200, Cell Signaling Technology, Danvers, MA, USA) and the monoclonal anti-NR4A3 (NOR-1) antibody (clone H-7, 1:25, Santa Cruz Biotechnology, Inc, Dallas, TX, USA), applying the automated Leica Bond III staining system (Leica Biosystems, Nussloch, Germany). The Ventana Benchmark staining system (Oro Valley, AZ, USA) was applied for the following primary antibodies: p63 (clone 4A4, prediluted, Ventana, Oro Valley, AZ, USA), p40 (clone BC24, 1:100, Zytomed Systems, Berlin, Germany), panTRK (clone EPR17341, 1:100, Abcam, Cambridge, UK), CD117 (clone YR145, 1:200, Cell Marque Lifescreen Ltd., Rocklin, CA, USA), Ki-67 (clone 30-9, prediluted, Ventana, Oro Valley, AZ, USA), S100 (polyclonal, 1:2000, DAKO A/S, Jena, Germany), DOG-1 (clone SP31, 1:50 Invitrogen, Carlsbad, CA, USA).

Data analysis

For the SalvGlandDx panel, the sequencing output bcl files were converted to fastq format and analyzed by the Archer analysis software (ArcherDX, Boulder, CO, USA). Fusion calls were considered positive when they had at least three unique reads, five unique start sites and 10% reads covering the breakpoint. Mutation calls were considered positive when they had at least five reads covering the mutant allele, three unique start sites and at least 5% mutant allele frequency. For expression analysis, the Archer analysis software normalizes the expression of the panel genes to the average expression of four control genes. Relative gene expression is then visualized in a heat map and displayed as numerical values.

For analysis of the Oncomine Assays, the IonReporter software (ThermoFisher Scientific, Waltham, MA, USA) was used with the generic filter settings.

Sanger sequencing results were analyzed using visual inspection of the DNA sequence.

Validation cohort (Table 2)

The cohort consisted of 32 FFPE samples (including three cell block specimen), mostly from salivary gland tumors. If salivary gland tumors with a certain alteration were not available, tests were applied to material from tumors with similar alterations. Moreover, the Archer SureShot sequencing controls (positive and negative control for ALK-RET-ROS1 fusions, ArcherDX, Boulder, CO, USA), were included.

Statistical analysis

Student's t-test was performed using GraphPad prism 8.0 to compare the *NR4A3* normalized expression values between the different groups. A P value < 0.05 was considered statistically significant. Receiver operating characteristic (ROC) curve analysis was performed using IBM SPSS Statistics 26.

Ethics statement

All patients, whose material was collected after 2015 signed a written informed consent for further use of their tissue and data. The current project is covered by approval from the local ethics review board (Kantonale Ethikkommision Zürich (BASEC-Nr. 2020-01663)), including a waiver for further material use collected prior to 2016.

Results

Panel validation

To validate our custom designed SalvGlandDx panel, we used a cohort of 34 samples, including two sequencing controls (Table 2) with alterations previously detected by current standard techniques for the different alterations (FISH, Sanger sequencing, immunohistochemistry, NGS). All samples passed the QC criteria set by the Archer analysis software.

Fusion analysis

Tumors with known fusions were available from 14 patients. Known fusions originate from FISH in five cases, NGS in five cases (Oncomine Focus or Comprehensive Assay v3, or Archer FusionPlexSarcoma panel), FISH plus NGS in one case and FISH plus IHC in one case. One case with *NTRK1* fusion and one case with a *NUTM1* fusion was confirmed by immunohistochemistry. Furthermore, the SureShot sequencing controls (positive and negative control for ALK-RET-ROS1 fusions) were used.

Table 2

Validation cohort.

Sample	Entity
SG-4	Adenocarcinoma NOS / potential spectrum microsecretory adenocarcinoma
SG-14	Polymorphous adenocarcinoma, cribriform variant / CASG
SG-17	Adenoid-cystic carcinoma, high-grade transformation
SG-24	Polymorphous adenocarcinoma, classical variant
SG-25	Clear cell carcinoma
SG-26	Polymorphous adenocarcinoma, classical variant
SG-29	Acinic cell carcinoma
SG-32	Adenoid-cystic carcinoma
SG-35	Epithelial-myoepithelial carcinoma, solid-oncocytic variant (published before) [53]
SG-36	Acinic cell carcinoma
SG-37	Acinic cell carcinoma
SG-38	Acinic cell carcinoma
SG-39	Acinic cell carcinoma
SG-41	Acinic cell carcinoma
SG-42	Secretory carcinoma
SG-44	Pleomorphic adenoma
SG-46	Adenoid-cystic carcinoma
SG-49	Adenocarcinoma NOS
SG-51	Mucoepidermoid carcinoma, oncocytic variant (OMEC)
SG-66	Carcinoma ex pleomorphic adenoma, minimal invasive
SG-68	Acinic cell carcinoma, high-grade transformation
SG-79	Epithelial-myoepithelial carcinoma, high-grade transformation
SG-84	Basal cell adenoma
SG-85	Acinic cell carcinoma, high-grade transformation
VD-1	Melanoma
VD-2	Melanoma
VD-3	Lung adenocarcinoma
VD-4	Lung adenocarcinoma
VD-5	NUT carcinoma
VD-6	NUT carcinoma
VD-7	Basal cell carcinoma of the skin
VD-8	Lipofibromatosis-like neural tumor
NEG	Archer SureShot negative control
POS	Archer SureShot positive control

SG = Salivary gland tumor, CASG = Cribriform adenocarcinoma of salivary gland, VD = Validation sample, NEG = negative control, POS = positive control

All known fusions were detected using the SalvGlandDx panel (Table 3). Furthermore, fusion partners from genes shown to be rearranged in FISH could be determined.

Mutation analysis

To validate the SalvGlandDx panel for mutation analysis, we used eleven tumors with known mutations, previously detected by Sanger sequencing (3 cases) and amplicon-based DNA sequencing with Oncomine panels (8 cases). Furthermore, the SureShot sequencing controls (positive and negative control) were included, as their backbone cell line HTC-116 has known mutations in *CTNNB1, KRAS* and *PIK3CA* that are covered by the SalvGlandDx target region. With the SalvGlandDx panel, we were able to detect all mutations (Table 4).

Recurring variants in *PIK3CA* (p.S514Kfs*2) and *PRKD3* (p.D304=) that were detected in the majority of all samples were flagged as artifacts. Moreover, several variants in *EWSR1*, one variant in *MYBL1* and one variant in *MAML2* occurred in more than one sample, however not in the majority of samples. All of them were variants of unknown significance and were therefore not further investigated.

Gene expression analysis

Eight acinic cell carcinomas (six classical and two with high-grade transformation) and one secretory carcinoma (negative control) were stained with the NR4A3 antibody. All eight acinic cell carcinomas were positive (Fig. 1A), while the secretory carcinoma showed no positive staining (Fig. 1B). Likewise, the visual as well as the numerical normalized expression values (NEV) for all eight cases were significantly increased, while the values for the negative control were low. Moreover, we compared the normalized expression values of all 25 salivary gland neoplasms of the validation cohort and found a clear difference between positive (mean: NEV = 5.72 ± 1.48) and negative (mean: NEV = 0.1 ± 0.14) samples ($P < 0.0001$, *t*-test, Fig. 1C). A ROC curve analysis yielded an area under the curve (AUC) = 1 with a sensitivity and specificity of 100% at an optimal discriminating cutoff of NEV = 2.32. Furthermore, visual inspection of the heatmap clearly distinguished positive and negative cases (Fig. 1D).

Three samples from our validation cohort originated from cytological specimen, showing that the panel is suitable to process not only tissue biopsies but also material from cell block specimen of fine needle aspirations (SG-51: *CRTC3-MAML2* fusion, SG-84: *CTNNB1* mutation, SG-85: *NR4A3* expression)

Table 3

Validation of known fusions.

Sample	Standard Diagnostic Method	Alteration Standard Diagnostic Method	Alteration SalvGlandDx
SG-4	FISH (*SS18*)	*SS18* rearrangement	*SS18-ZBTB7A*
SG-17	Amplicon sequencing (OCA)	*MYB-NFIB*	*MYB-NFIB*
SG-25	FISH (*EWSR1*)	*EWSR1* rearrangement	*EWSR1-ATF1*
SG-32	FISH (*MYBL1*)	*MYBL1* rearrangement	*MYBL1-NFIB*
SG-42	IHC (panTRK), FISH (*ETV6*)	panTRK+ *ETV6* rearrangement	*ETV6-NTRK3*
SG-44	Amplicon sequencing (OCA)	*FGFR1-PLAG1*	*FGFR1-PLAG1*
SG-46	FISH (*MYB*)	*MYB* rearrangement	*MYB-NFIB*
SG-49	Customized Archer® FusionPlex Sarcoma panel FISH (*NTRK2*)	*ZCCHC7-NTRK2* *NTRK2* rearrangement	*ZCCHC7-NTRK2*
SG-51	FISH (*MAML2*)	*MAML2* rearrangement	*CRTC3-MAML2*
SG-66	Archer® FusionPlexSarcoma panel	*HMGA2-WIF1*	*HMGA2-WIF1*
VD-4	Amplicon sequencing (OFA)	*KIAA1468-RET*	*KIAA1468-RET*
VD-5	Amplicon sequencing (OCA)	*WHSC1L1*(*NSD3*)*-NUTM1*	*NSD3-NUTM1*
VD-6	IHC (NUT)	NUT+	*BRD4-NUTM1*
VD-8	IHC (panTRK)	panTRK+	*TPM3-NTRK1*
NEG	Sequencing Control	-	-
POS	Sequencing Control	*CCDC6-RET*	*CCDC6-RET*

SG = Salivary gland neoplasm, VD = Validation sample, NEG = negative control
POS = positive control, OFA = Oncomine Focus Assay, OCA = Oncomine Comprehensive Assay, IHC = Immunohistochemistry

Table 4

Validation of known mutations

Sample	Standard Diagnostic Method	Alteration STANDARD DIAGNOSTIC METHOD	Alteration SalvGlandDx
SG-14	Sanger sequencing	*PRKD1* p.E710D	*PRKD1* p.E710D
SG-17	Amplicon sequencing (OCA)	*PIK3CA* p.E545K	*PIK3CA* p.E545K
SG-24	Sanger sequencing	*PRKD1* p.E710D	*PRKD1* p.E710D
SG-26	Sanger sequencing	*PRKD1* p.E710D	*PRKD1* p.E710D
SG-35	Amplicon sequencing (OCA)	*HRAS* p.Q61R	*HRAS* p.Q61R
SG-79	Amplicon sequencing (OFA)	*AKT1* p.E17K	*AKT1* p.E17K
SG-84	Amplicon sequencing (OFA)	*CTNNB1* p.I35T	*CTNNB1* p.I35T
VD-1	Amplicon sequencing (OFA)	*BRAF* p.V600E	*BRAF* p.V600E
VD-2	Amplicon sequencing (OFA)	*NRAS* p.Q61K	*NRAS* p.Q61K
VD-3	Amplicon sequencing (OFA)	*KRAS* p.G12C	*KRAS* p.G12C
VD-7	Amplicon sequencing (OCA)	*SMO* p.L412F	*SMO* p.L412F
NEG	Sequencing Control	*CTNNB1* p.S45del, *KRAS* p.G13D, *PIK3CA* p.H1047R	*CTNNB1* p.S45del, *KRAS* p.G13D, *PIK3CA*. p.H1047R
POS	Sequencing Control	*CTNNB1* p.S45del, *KRAS* p.G13D, *PIK3CA* p.H1047R	*CTNNB1* p.S45del, *KRAS* p.G13D, *PIK3CA* p.H1047R

SG = Salivary gland neoplasm; VD = Validation sample; NEG = negative control; POS = positive control; OFA = Oncomine™ Focus Assay; OCA = Oncomine™ Comprehensive Assay

Practical application of SalvGlandDx panel on four unique cases

Case 1: Purely oncocytic mucoepidermoid carcinoma (OMEC)

The first case was a 33-years old male with a lump in the right parotid gland. Fine needle aspiration in our cytopathology department revealed a bland oncocytic neoplasm, rendering a broad differential diagnosis (Fig. 2A, inset). The SalvGlandDx panel was performed on the cellblock specimen and detected a rare *CRTC3-MAML2* fusion, highly specific to mucoepidermoid carcinoma. A MAML2 FISH showed >15% split signals corroborating the detected *MAML2* rearrangement (Fig. 2A, inset). After signing out the final diagnosis of OMEC, the preoperative consenting and surgical plan was adapted. The following resection specimen showed an infiltrative, purely oncocytic neoplasm with intersecting broad fibrous bands and focal eosinophilic secretions (Fig. 2A-B). Only miniscule areas of glandular differentiation with likewise intraluminal eosinophilic secretions could be observed (Fig. 2C), while mucocytes were completely absent

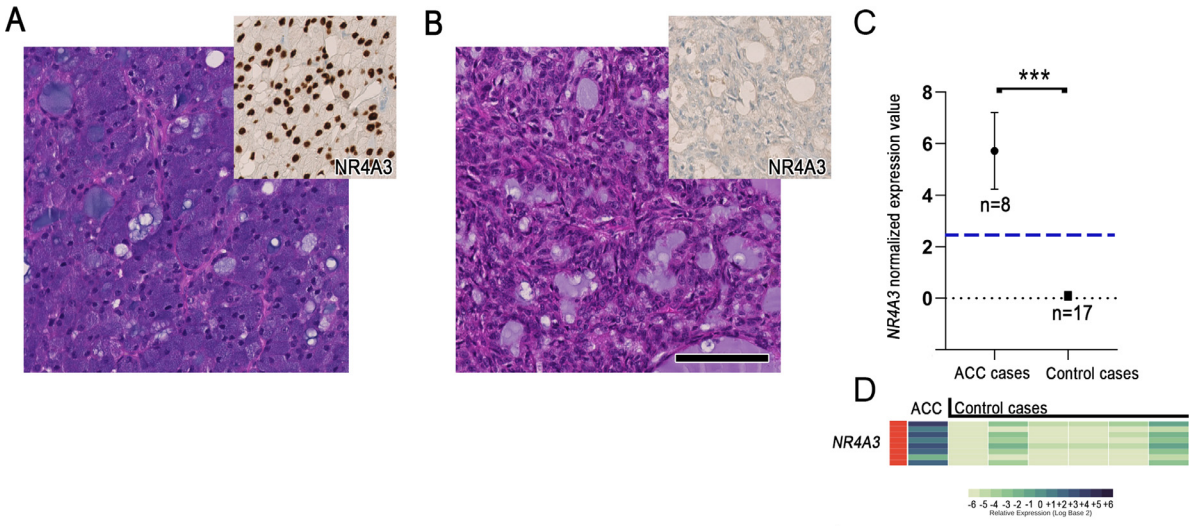

Fig. 1. High *NR4A3* mRNA expression levels are specific to acinic cell carcinoma (ACC). (A) shows a conventional acinic cell carcinoma with blue zymogen granules and strong nuclear expression of NR4A3 immunohistochemistry (inset). (B) illustrates secretory carcinoma as most important differential diagnosis, negative for nuclear NR4A3 (inset). The normalized expression values (NEV) in (C) depict a significant difference between the n=8 cases of acinic cell carcinomas (mean NEV = 5.72 ± 1.48) and the $n = 17$ remaining cases (mean NEV = 0.1 ± 0.14; $P < 0.0001$, t-test). The blue dotted line represents the optimal cutoff at NEV = 2.32, yielding an AUC = 1 with 100% sensitivity and specificity in a ROC curve analysis. (D) depicts representative heatmap of one NR4A3 positive case among negative cases. Scale bar 100 µm.

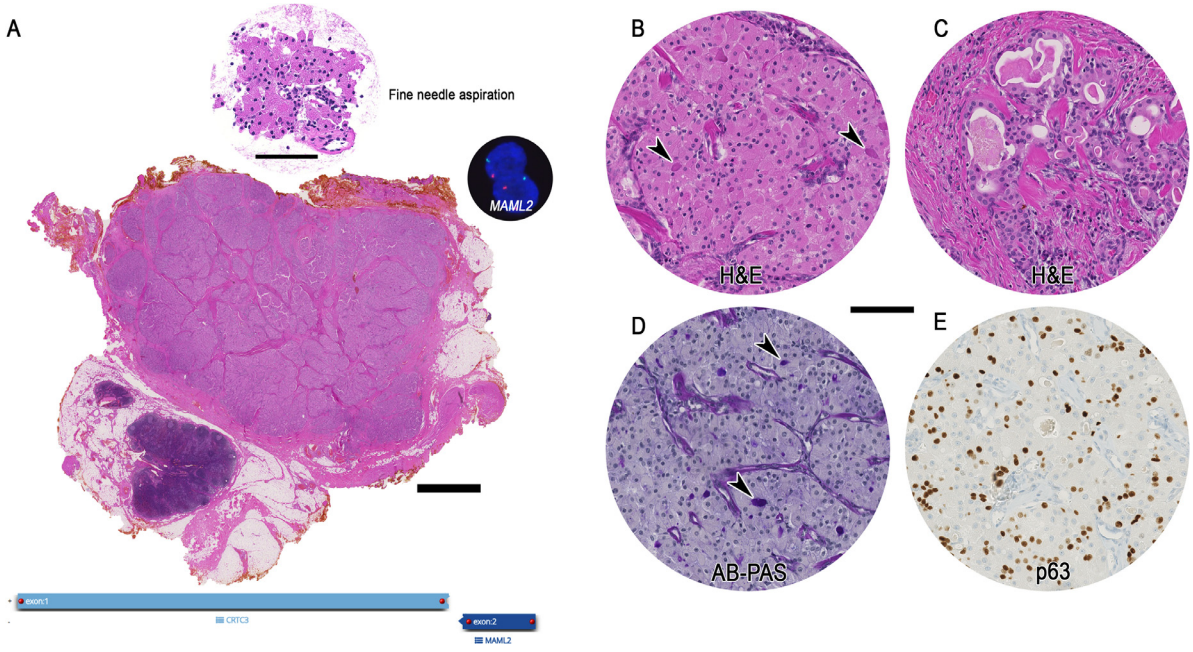

Fig. 2. Case 1**:** *CRTC3-MAML2* fused oncocytic mucoepidermoid carcinoma (OMEC). (A) shows bland oncocytic cells in the fine needle aspiration cellblock specimen (upper inset). *MAML2* FISH split signals can be appreciated in the corresponding inset. Resection specimen (below) depicts an infiltrating purely oncocytic neoplasia, intersecting the distinct fibrous bands. In (B) a magnification of the bland solid-oncocytic cell complexes is visualized with focal eosinophilic secretions (arrowheads). (C) shows very focal glandular differentiation with intraluminal secretions, however lacking the classical triphasic differentiation. In (D) the lack of typical alcianblue-positive mucocytes is illustrated, whereby the distinct spheroid violet reactivity was spatially correlating to the secretions (arrowheads). Immuohistochemical p63 expression was noted in a subset of cells (E). Scale bar 2.5 mm (overview), 100 µm (magnified insets).

(Fig. 2D). Furthermore, tumor manifestations were visible in close vicinity to peripheral nerve branches, however, without obvious perineural invasion. Immunhistochemical expression of p63 was positive in a subset of cells (Fig. 2E).

Case 2: Adenocarcinoma NOS with *NTRK2* fusion and multiphasic growth pattern

The second case was a 65 years-old male with a recurrent and infiltrating left parapharyngeal salivary gland tumor of exceptional morphology

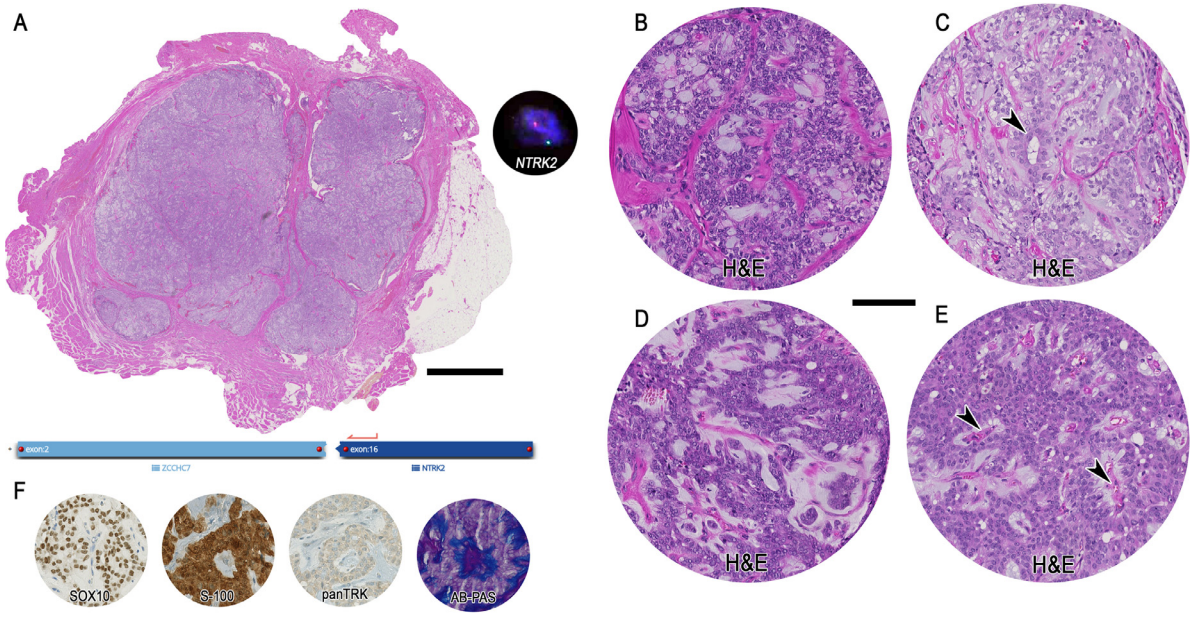

Fig. 3. Case 2: *ZCCHC7-NTRK2* fused adenocarcinoma NOS with multiphasic growth pattern. In (A) a parapharyngeal lobulated, cellular neoplasm is shown infiltrating into adjacent skeletal muscle. *NTRK2* FISH split signal can be observed (inset). Growth pattern encompassed microcystic (B), solid, epithel-myoepithelial carcinoma-like (arrowhead; C) and dissection of epithelioid cells in the distinct slate-gray background (D) pattern. In (E), tumoral pseudorosettes around vascular spaces are seen (arrowheads). Relevant immunohistochemical stains and accentuated alcianblue-PAS reactivity around the vascular spaces of the pseudorosettes is depicted in (F). Scale bar 2.5 mm (overview), 100 µm (magnified insets).

(Fig. 3A). The lobulated cellular mass showed dense intersecting and circumferential fibrous bands. The tumor cells were quite monomorphic and of one type, medium to large in size with clear chromatin, distinct nucleoli, eosinophilic and partially prominent clear cytoplasm with somewhat oncocytic aspect. Growth pattern encompassed a multiphasic microcystic, solid and cribriform morphology, with striking slate-grey extracellular deposits and stroma (Fig. 3B). Focal regions were reminiscent of epithelial-myoepithelial carcinoma with clearing of the more abluminal cells (*arrowhead*; Fig. 3C); however, no true biphasic cell type differentiation could be noted by immunohistochemistry. Furthermore, a segmental morphology with dissecting epithelioid complexes into the described background was observed (Fig. 3D). Another growth pattern showed marked pseudorosettes (*arrowheads*; Fig. 3E). Occasional mitotic figures were present. On immunohistochemistry SOX10 and S100 were diffusely expressed (Fig. 3F), corroborating a salivary gland origin. Mammaglobin, CD117, NR4A3, DOG1, p63, p40, PLAG1 and androgen receptor were negative (data not shown). GATA3 showed very weak single cell reactivity. Pan-cytokeratin, and CK7 were diffusely positive. Interestingly, Ki-67 showed a distinct pattern with confluent garland-like peripheral proliferation fronts, leaving an impression of a punched-out proliferation-negative geographical center (supplementary Fig. 1). PanTRK immunohistochemistry illustrated a very faint cytoplasmic and membranous reactivity, whereas Alcianblue-PAS staining depicted mucin depositions accentuated around the vascular spaces of the pseudorosettes (Fig. 3F). SalvGlandDx panel detected a *ZCCHC7-NTRK2* fusion, which has only been mentioned in an abstract, however without corresponding neoplasm type [54]. *NTRK2* FISH confirmed this finding (Fig. 3A, inset). Although features were reminiscent of pleomorphic adenoma, a true chondro-myxoid matrix could not be detected. Furthermore, no change in cell type or size was observed.

Case 3: Adenoid-cystic carcinoma with spindle cell and pseudoangiomatoid pattern

The third case describes an adenoid-cystic carcinoma with very uncommon morphology. This tumor was excised due to a submucosal mass on the left cheek of a 55 years-old male patient. Histology showed a quite well circumscribed cellular neoplasm (Fig. 4A) with mixed morphology. The main part of the neoplasm consisted of bland spindle cells embedded in a chondro-myxoid like stroma intermingled with mature fat (Fig. 4B). Furthermore, a pseudoangiomatoid pattern could be noticed, besides myxoid nodules with fibrosis (Fig. 4C-D). Limited foci showed an adenoid-cystic like morphology (Fig. 4E) and focal neural invasion and infiltration of the peripheral soft tissue. Immunohistochemistry for p40 was diffusely positive without noticeable biphasic differentiation, reminiscent of a myoepithelial overgrowth; whereas CD117 was virtually absent. Ki-67 proliferation index was very low (<5%; Fig. 4F). Although the tumor was resembling pleomorphic adenoma, the infiltrative pattern exceeded the classical observed features and rendered the differential diagnosis of carcinoma ex pleomorphic adenoma or unusual de novo adenoid-cystic carcinoma. Panel sequencing revealed a *MYBL1-NFIB* fusion, which was confirmed by corresponding split signals in *MYBL1* FISH (Fig. 3A, inset). No rearrangement of *PLAG1* or *HMGA2* was detected. Final diagnosis was adenoid-cystic carcinoma with spindle cell and pseudoangiomatoid differentiation, mimicking pleomorphic adenoma.

Case 4: *SS18-ZBTB7A* rearranged low-grade adenocarcinoma

This case derives from the parotid gland of a 60 years-old male, who underwent surgery due to a squamous cell carcinoma in the parotid gland. Besides, the resection specimen revealed a 7 mm diffusely infiltrating adenocarcinoma (Fig. 5A) with bland solid, cribriform, tubular and trabecular epithelial complexes (Fig. 5B-D). Focal oncocytic differentiation was observed, including rhabdoid- / histiocytoid-like single cells dissecting into the stroma (Fig. 5E). A prominent sclerotic stroma was evident in the background, while also distinct intraluminal bubbly secretions were noted (Fig. 5E). Immunohistochemistry showed diffuse expression of SOX10, while DOG-1 showed an apical-membranous pattern, indicative of an intercalated duct differentiation. S100 was diffusely expressed in a heterogeneous pattern. A p40 staining was largely negative, including very limited areas of a biphasic pattern with single positive abluminal cells (Fig. 5F).

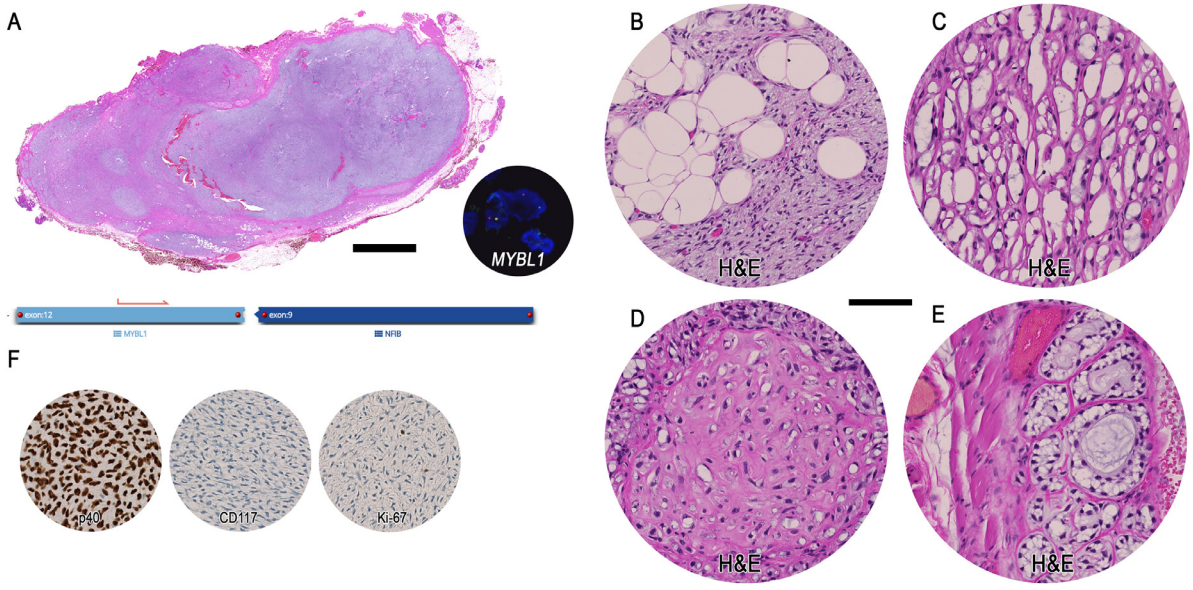

Fig. 4. Case 3: *MYBL1-NFIB* fused adenoid-cystic carcinoma with largely unusual morphology. (A) shows a quite well circumscribed cellular neoplasm. *MYBL1* FISH shows split signals (inset). In (B) the bland spindle cells mixed with mature (probably infiltrated) fat and the prominent myxoid background is depicted. The pseudoangiomatoid pattern is represented in (C) with capillary-like structures. The fibro-myxoid nodules can be appreciated in (D) and (E) shows very limited foci of more conventional cribriform morphology. The diffuse p40 expression with monophasic pattern is visualized in (F), with CD117 negativity and very low Ki-67 proliferation index. Scale bar 2.5 mm (overview), 100 µm (magnified insets).

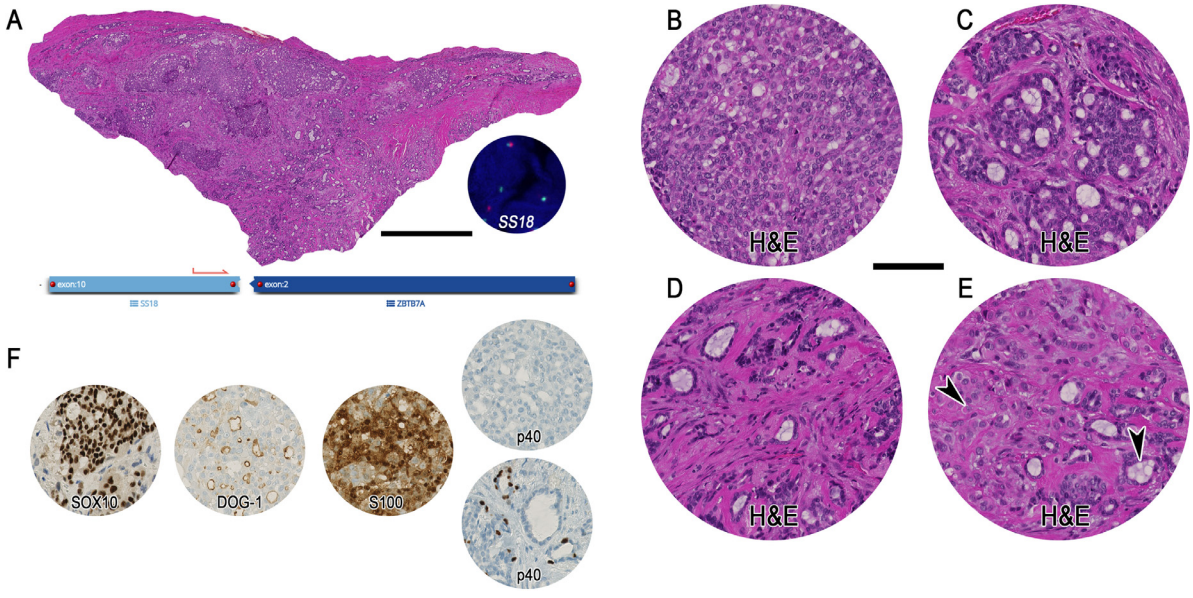

Fig. 5. Case 4: *SS18-ZBTB7A* fused low-grade adenocarcinoma. (A) shows diffusely infiltrating adenocarcinoma with split signals in *SS18* FISH (inset). The magnification in (B) illustrates the solid growth of medium-sized atypical cells including subtle nucleoli and slightly oncocytic differentiation. In (C) the cribriform ductal differentiation is depicted, whereas (D) pictures the small irregular tubular complexes within a sclerotic stroma, reminiscent of tubular breast cancer. (E) outlines the more oncocytic single cells with a histiocytoid / rhabdoid differentiation (left arrowhead). The right arrowhead points to the intraglandular bubbly secretions. The relevant immunhistochemical stainings are shown in (F), whereas the lower p40 staining describes the focal biphasic differentiation in contrast to the negative upper staining representative for most of the tumor. Scale bar 2.5 mm (overview), 100 µm (magnified insets).

SalvGlandDx panel showed a *SS18-ZBTB7A* fusion, corroborated by positive *SS18* FISH (Fig. 5A, inset). The morphology and molecular profile matched with the single other published case, which has been reported as potential spectrum of the recently described microsecretory adenocarcinoma [22].

Identification of novel fusions involving the PRKD *genes*

To identify fusion partners of the investigated *PRKD* genes, six cases of polymorphous adenocarcinoma including cribriform variant / cribriform adenocarcinoma of salivary gland (CASG) were identified from our archive

Table 5

Clinicopathological features of investigated polymorphous adenocarcinomas (PAC) including cribriform variant / cribriform adenocarcinoma of salivary gland (CASG).

Case	1	2	3	4	5	6
Age	33	54	74	34	84	67
Sex	f	m	f	m	f	m
Localization	Buccal	Hard / soft palate	Buccal, maxillary sinus	Soft palate	Parotid gland	Soft palate
Size	1.3 cm	0.9 cm	5.5 cm	1.1 cm	2.4 cm	0.5 cm
Morphology	PAC, classical variant	PAC, classical variant	PAC, cribriform variant / CASG with basaloid features	PAC, cribriform variant / CASG	PAC, cribriform variant / CASG	PAC, classical variant
Molecular aberration	*PRKD1* p.E710D	*PRKD1* p.E710D	*PRKD1* p.E710D	*PRKAR2A-PRKD1*	*SNX9-PRKD1*	*ATL2-PRKD3*
Perineural invasion	yes	yes	yes	yes	yes	yes
Metastases	no	no	no	yes, Neck, Level II-III, 14 years after primary	no	no
Therapy	Resection	Resection	Resection, adjuvant radiotherapy	Resection, adjuvant radiotherapy	Resection, adjuvant radiotherapy	Resection
Follow-up	NED, 74 months	NED, 39 months	NED, 12 months	NED, 243 months	NED, 16 months	NED, 3 months

NED = no evidence of disease

including consult cases and subjected to sequencing with the SalvGlandDx panel. Clinicopathological overview is depicted in Table 5.

Three cases (50%) with an origin in the oral mucosa showed an activating *PRKD1* p.E710D mutation, of which two cases showed a classical polymorphous (low-grade) morphology (Fig. 6A). One case was a large polypoid tumor of 5.5 cm in the maxillary sinus and showed largely solid differentiation including prominent nuclear clearing, compatible with cribriform variant /CASG. Of note, besides focal typical glomeruloid growth, this case showed an uncommon basaloid morphology with extracellular basal membrane-like material reminiscent of basal cell adenocarcinoma (Fig. 6B, inset). The other three cases showed *PRKD* gene fusions. One case showed a *PRKAR2A-PRKD1* fusion and was metastasized to the neck lymph nodes 14 years after the primary tumor was resected from the soft palate. Morphology encompassed typical features of cribriform variant / CASG with solid, glomeruloid and focal papillary growth (case not shown). Another case harbored a *SNX9-PRKD1* rearrangement and likewise represented a typical solid, glomeruloid and focal papillary architecture with calcifications as described in cribriform variant / CASG [55] (Fig. 6C). Remarkably, this tumor was located in the parotid gland without clinical evidence for any other manifestation. The remaining case showed an *ATL2-PRKD3* fusion, however, was depicting a classical monophasic low-grade appearance similar to the first two cases with focal perineural invasion in the oral mucosa (Fig. 6D).

Discussion

With the validation of the known alterations in our cohort, we were able to design a custom NGS panel that facilitates the diagnosis and classification of salivary gland neoplasms with one single test. Well-known fusions as well as hotspot mutations and elevated gene expression of *NR4A3* could reliably be detected not only in histological FFPE tissue, but also in cell block specimen of fine needle aspirations. The latter in particular may allow a more precise diagnosis and alleviate the need for core needle biopsy and/or incisional biopsy. To our knowledge this is the first validated panel that includes all relevant genes to detect specific alterations, including mutations, fusions and gene expressions on RNA level. While usually only single alterations can be tested at the time (e.g. FISH, IHC, Sanger sequencing), some commercially available NGS panels cover certain genes, however, not all of them within one assay.

Besides the detection of relevant alterations for salivary gland neoplasm diagnosis and classification, our panel can reliably detect therapeutic targets, such as *NTRK* fusions. Here, *NTRK* inhibitors (e.g. larotrectinib, entrectinib) were recently shown to be effective in patients with *NTRK* fusions [56, 57]. According to the ESMO guidelines, testing with an RNA-based NGS assay is preferred for these alterations [58].

High expression levels of *NR4A3* were specifically associated with acinic cell carcinoma in our study, as described by Haller *et al.* [5]. In particular on FNA specimen, the diagnosis of acinic cell carcinoma can be hampered by high similarity to normal acinic cells [59]. Moreover, cases with high-grade morphology might not show the typical features. Our two cases with high-grade transformation could correctly be assigned to acinic cell carcinoma by the panel results, corroborated by positive NR4A3 immunohistochemistry. One case could already be diagnosed on the FNA specimen guided by high *NR4A3* expression levels detected by the SalvGlandDx panel. The (high-grade) morphology on the FNA specimen was not specific; however, the diagnosis was confirmed on the histological specimen showing partial obvious classical (low-grade) differentiation.

Case 1 showed an intriguing oncocytic mucoepidermoid carcinoma (OMEC), lacking the typical mucocytes and triphasic differentiation as recently described by Skalova *et al.* [60] and one similar case by Todorovic *et al.* [61]. The *CRTC3-MAML2* fusion is highly specific to mucoepidermoid carcinoma [18], whereas the detection on the cellblock specimen combined with the oncocytic morphology was sufficient for this diagnosis. Current data suggest that (purely) oncocytic and sclerosing variant of MEC are most likely low-grade neoplasms [62, 63], which seem to show a more indolent biological behavior. However, one has to be aware that current grading schemes (e.g. AFIP and Brandwein-Gensler) might lead to a distinct appraisal [60]. Future

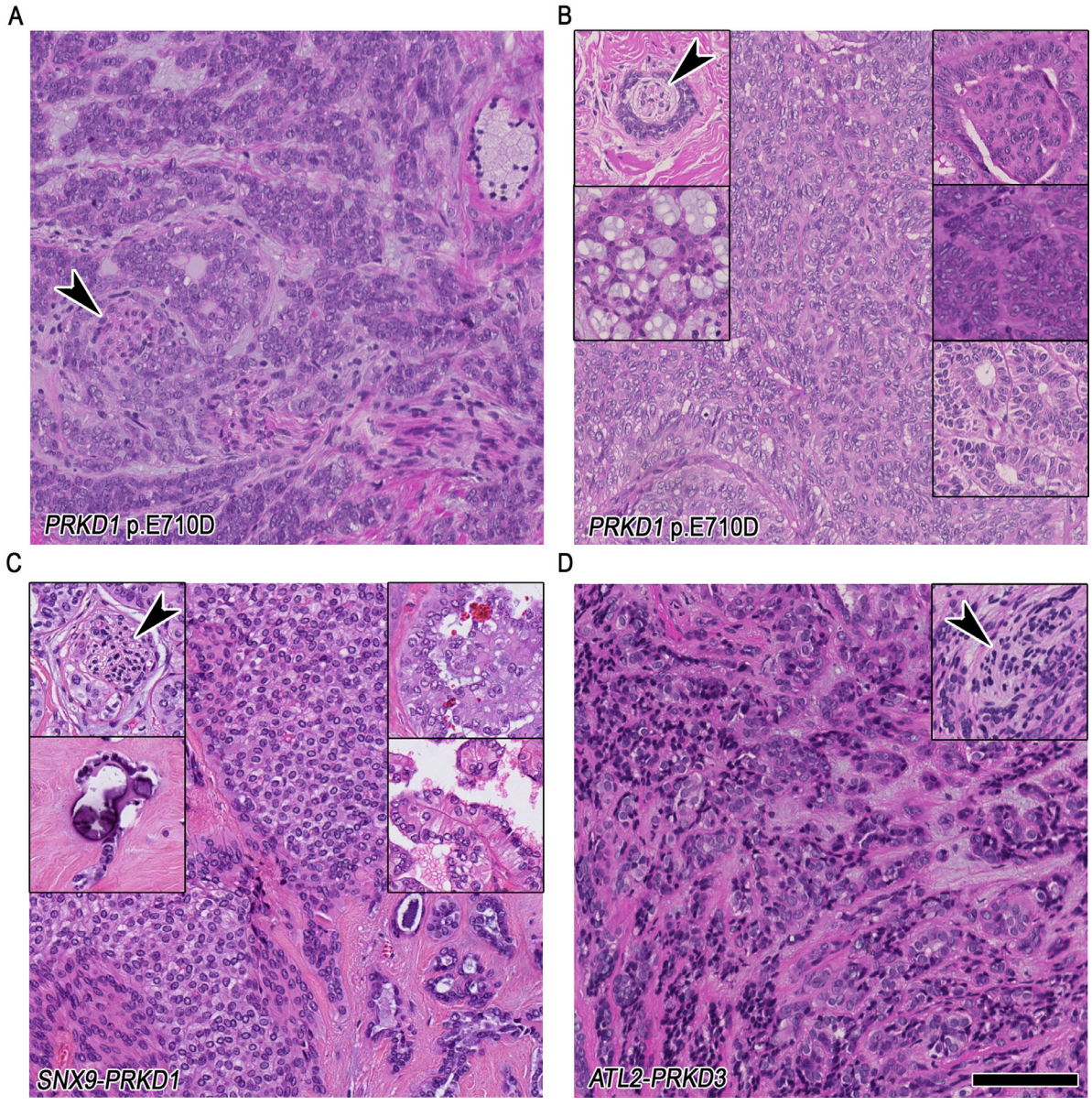

Fig. 6. Morphological comparison of *PRKD1* p.E710D mutated and *PRKD1/PRKD3* rearranged polymorphous adenocarcinoma (PAC) / cribriform adenocarcinoma of salivary gland (CASG). (A) shows classical monomorphic tubular and trabecular PAC complexes with diffuse infiltrative pattern including targetoid perineural invasion (arrowhead), a slate-grey stroma and an underlying *PRKD1* p.E710D mutation. In (B) another case with *PRKD1* p.E710D mutation derived from a maxillary sinus polypoid lesion is depicted, however illustrating a solid differentiation with prominent nuclear clearing reminiscent of papillary thyroid carcinoma, compatible with cribriform variant / CASG. In the insets focal perineural invasion (arrowhead) is shown and different growth patterns encompassing cribriform, glomeruloid, basaloid jigsaw-like and ductal-like. (C) illustrates the typical morphological spectrum of a (parotid gland) cribriform variant / CASG harboring a *SNX9-PRKD1* fusion, including nuclear clearing of solid tumor complexes, perineural invasion (arrowhead), glomeruloid and papillary growth pattern as well as focal calcifications (insets). Of note, the stroma is sclerotic. (D) depicts a morphological similar case to (A), including targetoid perineural invasion (arrowhead) and slate-grey stroma, however harboring *ATL2-PRKD3* fusion. Scale bar 100 µm.

data will be needed to clarify this issue and potentially grade these subentities separately.

The second case revealed a novel *ZCCHC7-NTRK2* fusion, which could be verified independently in other laboratories using NGS panel and a break-apart FISH assay. That approach shows, that directed molecular testing can, albeit in rare instances, reveal targetable alterations. The uncommon mixed morphology was not assignable to a known entity. The immunohistochemical phenotype, encompassing SOX10 and S100 co-expression, corroborated the diagnosis of a salivary gland neoplasm. Although the tumor showed areas reminiscent of pleomorphic adenoma (PA), including the variety of growth patterns and distinct background, no true chondro-myxoid matrix or fibrous (pseudo)capsule could be observed. Furthermore, the cell type was overall too monomorphic, large and atypical in comparison to a conventional PA. The observed infiltrative growth pattern on the resection specimen, without a typical change of cell type or cell overgrowth rather represents a distinct clonal entity than a carcinoma ex pleomorphic adenoma in our view. Despite similarities to a myoepithelial-like immunophenotype [64], the presence of abundant ductal structures

did not admit diagnosis of a (secretory) myoepithelial carcinoma [65, 66]. An uncommon variant of secretory carcinoma, involving commonly *ETV6-NTRK3* fusions, could not be diagnosed due to a distinct morphology, molecular and immunohistochemical profile (e.g. mammaglobin negative) [6]. Altogether, the observed cell type shows similarities to striated ducts in normal salivary gland tissue, however the immunophenotypes cannot be matched [67]. Besides, the distinct background and single cell type showing different growth patterns could lead to the differential diagnosis of polymorphous adenocarcinoma; however, the comprehensive profile does not fit in this category [68]. *NTRK2* fusions are extremely rare and even less common than *NTRK1* and *NTRK3* fusions. In two recently published clinical trials investigating the NTRK inhibitors entrectinib and larotrectinib in solid tumors, only one out of 54 and 55 participants, respectively, harbored a *NTRK2* fusion without mentioning the tumor entity [56, 57]. We were not able to find a specific report of a *NTRK2* fused salivary gland neoplasm in the literature at the current time. Morphology encompassed a single cell type with multiphasic and infiltrative growth pattern, whereas further cases have to elucidate a potential recurrent nature of this outstanding type of neoplasm.

The third case showed a very uncommon morphology, which could lead to a misinterpretation of pleomorphic adenoma. Parallel sequencing of the fusion genes with the described panel could thereby help to further corroborate a carcinoma ex pleomorphic adenoma, which typically harbors *PLAG1* or *HMGA2* fusions [69, 70]. *MYBL1-NFIB* rearrangements can be detected in up to 24% of adenoid-cystic carcinoma and are highly specific for this tumor entity [15, 16]. Overall, this fusion corroborates the diagnosis of adenoid-cystic carcinoma although the morphology was largely unusual. The molecular finding is in line with a recently published similar case, however obscuring its origin by illustrating squamous differentiation [61].

The fourth case was initially classified as adenocarcinoma NOS, as it did not fit to a known category. Sequencing revealed a *SS18-ZBTB7A* fusion, which has been recently described in a potential spectrum of microsecretory adenocarcinoma (MSA), typically harboring *MEF2C-SS18* fusions and occurring in the oral cavity [22]. Interestingly, it was similarly small (< 1 cm) and located in the parotid gland likewise as the only case with this fusion described by Bishop *et al.* [22]. Our case showed the identical fusion (*SS18* exon 10, *ZBTB7A* exon 2), a similar morphological and immunohistochemical profile (largely negative for p63 and p40). In addition, we describe a DOG1 expression, indicative of a potential intercalated duct differentiation [71]; however, no information about DOG1 expression in bona fide MSA is available. Due to an identical morphological, immunohistochemical and molecular profile, our case corroborates that this tumor type is a recurrent finding. However, further cases have to elucidate whether this is a genuine spectrum of MSA or a separate entity sharing some features with MSA.

PRKD1 mutations were specific to the spectrum of polymorphous adenocarcinoma (PAC). Most of the classical PAC did show a recurrent *PRKD1* p.E710D mutation, whereas one (metastasized) cribriform variant / CASG did show a previously undescribed *PRKAR2A-PRKD1* fusion. However, one case of a classical PAC did show an *ATL2-PRKD3* fusion and one case of a non-metastasized cribriform variant / CASG with uncommon basaloid features harbored a *PRKD1* p.E710D mutation, corroborating the findings from Sebastiao *et al.* that the type of aberration is not entirely specific for classical PAC or cribriform variant / CASG [43]. Moreover, the case harboring the *SNX9-PRDK1* fusion was located in the parotid gland without evidence of other manifestations, underscoring the previous finding that this entity can also occur rarely in the major salivary glands [21]. Polymorphous adenocarcinoma is rarely observed in the sinonasal tract [72], whereas cribriform variant /CASG has to the best of our knowledge not been described to involve the maxillary sinus, yet. Morphological classification of these neoplasms has been difficult among a large multicenter study [21]. However, molecular analysis can help to assign a certain tumor with uncommon morphology or on a small biopsy /FNA to the described spectrum. Mutations in the other investigated genes are generally less specific. However, there are only exceedingly rare reports of a benign salivary gland neoplasm harboring an activating *HRAS* mutation (in this case: sialadenoma papilliferum) [47]. With a compatible morphology, *HRAS* mutation is strongly underscoring epithelial-myoepithelial carcinoma, even in uncommon variants [4].

We envision the SalvGlandDx panel as a useful all-in-one tool to diagnose and classify salivary gland neoplasms. With this panel, we can corroborate the findings from Todorovic *et al.*, who showed the importance of next generation sequencing in salivary gland neoplasms from different aspects [61]. The great advantage is thereby the simultaneous capturing of aberrant expression, gene mutations and fusions with the only need of RNA extraction, also reliably working on FFPE cell block specimen. One drawback might be uncovered individual fusions, such as *ALK* rearrangements, recently described in a small subset of intraductal carcinoma [73]. However, due to the design of the Archer FusionPlex technology, the panel can easily be amended in the future to include relevant emerging genes; however, keeping it as small as possible to optimize utilization on the sequencer. Nevertheless, this assay can significantly help to proper classify most of the salivary gland neoplasms, as it includes most of the recurrent gene aberrations known to date. Furthermore, it is able to simultaneously reveal potential molecular therapeutic targets such as *NTRK* and *RET* fusions, and can be applied on cellblock specimen of minimal invasive fine needle aspiration.

Acknowledgments

The authors thank Susanne Dettwiler and Fabiola Prutek from the institutional biobank, the laboratory for in situ techniques, the IT support, Marion Bawohl and the laboratory for Sanger sequencing, all from the Department of Pathology and Molecular Pathology at the University Hospital Zurich for excellent technical assistance.

Supplementary materials

Supplementary material associated with this article can be found, in the online version, at doi:10.1016/j.neo.2021.03.008.

References

1 Nix JS, Rooper LM. Navigating small biopsies of salivary gland tumors: a pattern-based approach. *Journal of the American Society of Cytopathology* 2020;**9**:369–82. doi:10.1016/j.jasc.2020.06.004.

2 Pusztaszeri M, Rossi ED, Baloch ZW, Faquin WC. Salivary Gland Fine Needle Aspiration and Introduction of the Milan Reporting System. *Advances in Anatomic Pathology* 2019;**26**:84–92. doi:10.1097/PAP.0000000000000224.

3 Skálová A, Stenman G, Simpson RHW, Hellquist H, Slouka D, Svoboda T, Bishop JA, Hunt JL, Nibu K-I, Rinaldo A, et al. The Role of Molecular Testing in the Differential Diagnosis of Salivary Gland Carcinomas. *Am J Surg Pathol* 2018;**42**:e11–27. doi:10.1097/PAS.0000000000000980.

4 Urano M, Nakaguro M, Yamamoto Y, Hirai H, Tanigawa M, Saigusa N, Shimizu A, Tsukahara K, Tada Y, Sakurai K, et al. Diagnostic Significance of HRAS Mutations in Epithelial-Myoepithelial Carcinomas Exhibiting a Broad Histopathologic Spectrum. *Am J Surg Pathol* 2019;**43**:984–94. doi:10.1097/PAS.0000000000001258.

5 Haller F, Bieg M, Will R, Körner C, Weichenhan D, Bott A, Ishaque N, Lutsik P, Moskalev EA, Mueller SK, et al. Enhancer hijacking activates oncogenic transcription factor NR4A3 in acinic cell carcinomas of the salivary glands. *Nat Commun* 2019. doi:10.1038/s41467-018-08069-x.

6 Skálová A, Vanecek T, Sima R, Laco J, Weinreb I, Perez-Ordonez B, Starek I, Geierova M, Simpson RHW, Passador-Santos F, et al. Mammary Analogue Secretory Carcinoma of Salivary Glands, Containing the ETV6-NTRK3 Fusion Gene: A Hitherto Undescribed Salivary Gland Tumor Entity. *The American Journal of Surgical Pathology* 2010;**34**:599–608. doi:10.1097/PAS.0b013e3181d9efcc.

7 Zito Marino F, Pagliuca F, Ronchi A, Cozzolino I, Montella M, Berretta M, Errico ME, Donofrio V, Bianco R, Franco R. NTRK Fusions, from the Diagnostic Algorithm to Innovative Treatment in the Era of Precision Medicine. *Int J Mol Sci* 2020. doi:10.3390/ijms21103718.

8 Asahina M, Saito T, Hayashi T, Fukumura Y, Mitani K, Yao T. Clinicopathological effect of PLAG1 fusion genes in pleomorphic adenoma and carcinoma ex pleomorphic adenoma with special emphasis on histological features. *Histopathology* 2019;**74**:514–25. doi:10.1111/his.13759.

9 Skálová A, Agaimy A, Vanecek T, Banecková M, Laco J, Ptáková N, Šteiner P, Majewska H, Biernat W, Corcione L, et al. Molecular Profiling of Clear Cell Myoepithelial Carcinoma of Salivary Glands With EWSR1 Rearrangement Identifies Frequent PLAG1 Gene Fusions But No EWSR1 Fusion Transcripts. *The American Journal of Surgical Pathology* 2021;**45**:1–13. doi:10.1097/PAS.0000000000001591.

10 Dalin MG, Katabi N, Persson M, Lee K-W, Makarov V, Desrichard A, Walsh LA, West L, Nadeem Z, Ramaswami D, et al. Multi-dimensional genomic analysis of myoepithelial carcinoma identifies prevalent oncogenic gene fusions. *Nat Commun* 2017. doi:10.1038/s41467-017-01178-z.

11 El Hallani S, Udager AM, Bell D, Fonseca I, Thompson LDR, Assaad A, Agaimy A, Luvison AM, Miller C, Seethala RR, et al. Epithelial-Myoepithelial Carcinoma: Frequent Morphologic and Molecular Evidence of Preexisting Pleomorphic Adenoma, Common HRAS Mutations in PLAG1-intact and HMGA2-intact Cases, and Occasional TP53, FBXW7, and SMARCB1 Alterations in High-grade Cases. *Am J Surg Pathol* 2018;**42**:18–27. doi:10.1097/PAS.0000000000000933.

12 Afshari MK, Fehr A, Nevado PT, Andersson MK, Stenman G. Activation of PLAG1 and HMGA2 by gene fusions involving the transcriptional regulator gene NFIB. *Genes, Chromosomes and Cancer* 2020;**59**:652–60. doi:10.1002/gcc.22885.

13 Persson F, Andrén Y, Winnes M, Wedell B, Nordkvist A, Gudnadottir G, Dahlenfors R, Sjögren H, Mark J, Stenman G. High-resolution genomic profiling of adenomas and carcinomas of the salivary glands reveals amplification, rearrangement, and fusion of HMGA2. *Genes, Chromosomes and Cancer* 2009;**48**:69–82. doi:10.1002/gcc.20619.

14 Wasserman JK, Dickson BC, Smith A, Swanson D, Purgina BM, Weinreb I. Metastasizing Pleomorphic Adenoma: Recurrent PLAG1/HMGA2 Rearrangements and Identification of a Novel HMGA2-TMTC2 Fusion. *The American Journal of Surgical Pathology* 2019;**43**:1145–51. doi:10.1097/PAS.0000000000001280.

15 Togashi Y, Dobashi A, Sakata S, Sato Y, Baba S, Seto A, Mitani H, Kawabata K, Takeuchi K. MYB and MYBL1 in adenoid cystic carcinoma: diversity in the mode of genomic rearrangement and transcripts. *Mod Pathol* 2018;**31**:934–46. doi:10.1038/s41379-018-0008-8.

16 Brayer KJ, Frerich CA, Kang H, Ness SA. Recurrent Fusions in MYB and MYBL1 Define a Common, Transcription Factor–Driven Oncogenic Pathway in Salivary Gland Adenoid Cystic Carcinoma. *Cancer Discov* 2016;**6**:176–87. doi:10.1158/2159-8290.CD-15-0859.

17 Fonseca FP, Filho MS, Altemani A, Speight PM, Vargas PA. Molecular signature of salivary gland tumors: potential use as diagnostic and prognostic marker. *Journal of Oral Pathology & Medicine* 2016;**45**:101–10. doi:10.1111/jop.12329.

18 Nakayama T, Miyabe S, Okabe M, Sakuma H, Ijichi K, Hasegawa Y, Nagatsuka H, Shimozato K, Inagaki H. Clinicopathological significance of the CRTC3–MAML2 fusion transcript in mucoepidermoid carcinoma. *Modern Pathology* 2009;**22**:1575–81. doi:10.1038/modpathol.2009.126.

19 Weinreb I, Piscuoglio S, Martelotto LG, Waggott D, Ng CKY, Perez-Ordonez B, Harding NJ, Alfaro J, Chu KC, Viale A, et al. Hotspot activating PRKD1 somatic mutations in polymorphous low-grade adenocarcinomas of the salivary glands. *Nature Genetics* 2014;**46**:1166–9. doi:10.1038/ng.3096.

20 Weinreb I, Zhang L, Tirunagari LM, Sung Y-S, Chen C-L, Perez-Ordonez B, Clarke BA, Skalova A, Chiosea SI, Seethala RR, et al. Novel PRKD gene rearrangements and variant fusions in cribriform adenocarcinoma of salivary gland origin. *Genes, Chromosomes and Cancer* 2014;**53**:845–56. doi:10.1002/gcc.22195.

21 Xu B, Barbieri AL, Bishop JA, Chiosea SI, Dogan S, Di Palma S, Faquin WC, Ghossein R, Hyrcza M, VY Jo, et al. Histologic Classification and Molecular Signature of Polymorphous Adenocarcinoma (PAC) and Cribriform Adenocarcinoma of Salivary Gland (CASG): An International Interobserver Study. *The American Journal of Surgical Pathology* 2020;**44**:545–52. doi:10.1097/PAS.0000000000001431.

22 Bishop JA, Weinreb I, Swanson D, Westra WH, Qureshi HS, Sciubba J, MacMillan C, Rooper LM, Dickson BC. Microsecretory Adenocarcinoma: A Novel Salivary Gland Tumor Characterized by a Recurrent: MEF2C-SS18: Fusion. *The American Journal of Surgical Pathology* 2019;**43**:1023–32. doi:10.1097/PAS.0000000000001273.

23 Andreasen S, Varma S, Barasch N, Thompson LDR, Miettinen M, Rooper L, Stelow EB, Agander TK, Seethala RR, Chiosea SI, et al. The HTN3-MSANTD3 Fusion Gene Defines a Subset of Acinic Cell Carcinoma of the Salivary Gland. *The American Journal of Surgical Pathology* 2019;**43**:489–96. doi:10.1097/PAS.0000000000001200.

24 Skálová A, Ptáková N, Santana T, Agaimy A, Ihrler S, Uro-Coste E, Thompson LDR, Bishop JA, Baněčkova M, Rupp NJ, et al. NCOA4-RET and TRIM27-RET Are Characteristic Gene Fusions in Salivary Intraductal Carcinoma, Including Invasive and Metastatic Tumors: Is „Intraductal" Correct? *Am J Surg Pathol* 2019;**43**:1303–13. doi:10.1097/PAS.0000000000001301.

25 Bishop JA, Nakaguro M, Whaley RD, Ogura K, Imai H, Laklouk I, Faquin WC, Sadow PM, Gagan J, Nagao T. Oncocytic Intraductal Carcinoma of Salivary Glands: A Distinct Variant with TRIM33-RET Fusions and BRAF V600E mutations. *Histopathology* 2020. doi:10.1111/his.14296.

26 Skálová A, Baneckova M, Thompson LDR, Ptáková N, Stevens TM, Brcic L, Hyrcza M, Michal MJ, Simpson RHW, Santana T, et al. Expanding the Molecular Spectrum of Secretory Carcinoma of Salivary Glands With a Novel VIM-RET Fusion. *The American Journal of Surgical Pathology* 2020;**44**:1295–307. doi:10.1097/PAS.0000000000001535.

27 Skalova A, Vanecek T, Martinek P, Weinreb I, Stevens TM, Simpson RHW, Hyrcza M, Rupp NJ, Baneckova M, Michal M, et al. Molecular Profiling of Mammary Analog Secretory Carcinoma Revealed a Subset of Tumors Harboring a Novel ETV6-RET Translocation: Report of 10 Cases. *Am J Surg Pathol* 2018;**42**:234–46. doi:10.1097/PAS.0000000000000972.

28 Rooper LM, Karantanos T, Ning Y, Bishop JA, Gordon SW, Kang H. Salivary Secretory Carcinoma With a Novel ETV6-MET Fusion: Expanding the Molecular Spectrum of a Recently Described Entity. *Am J Surg Pathol* 2018;**42**:1121–6. doi:10.1097/PAS.0000000000001065.

29 Antonescu CR, Katabi N, Zhang L, Sung YS, Seethala RR, Jordan RC, Perez-Ordoñez B, Have C, Asa SL, Leong IT, et al. EWSR1-ATF1 fusion is a novel and consistent finding in hyalinizing clear-cell carcinoma of salivary gland. *Genes, Chromosomes and Cancer* 2011;**50**:559–70. doi:10.1002/gcc.20881.

30 Vogels R, Baumhoer D, van Gorp J, Eijkelenboom A, Verdijk M, van Cleef P, Bloemena E, Slootweg PJ, Lohman B, Debiec-Rychter M, et al. Clear Cell Odontogenic Carcinoma: Occurrence of EWSR1-CREB1 as Alternative Fusion Gene to EWSR1-ATF1. *Head Neck Pathol* 2018;**13**:225–30. doi:10.1007/s12105-018-0953-z.

31 Chapman E, Skalova A, Ptakova N, Martinek P, Goytain A, Tucker T, Xiong W, Leader M, Kudlow BA, Haimes JD, et al. Molecular Profiling of Hyalinizing Clear Cell Carcinomas Revealed a Subset of Tumors Harboring a Novel EWSR1-CREM Fusion: Report of 3 Cases. *The American Journal of Surgical Pathology* 2018;**42**:1182–9. doi:10.1097/PAS.0000000000001114.

32 Rooper LM, Jo VY, Antonescu CR, Nose V, Westra WH, Seethala RR, Bishop JA. Adamantinoma-like Ewing Sarcoma of the Salivary Glands: A Newly Recognized Mimicker of Basaloid Salivary Carcinomas. *The American Journal of Surgical Pathology* 2019;**43**:187–94. doi:10.1097/PAS.0000000000001171.

33 Agaimy A, Fonseca I, Martins C, Thway K, Barrette R, Harrington KJ, Hartmann A, French CA, Fisher C. NUT Carcinoma of the Salivary Glands: Clinicopathologic and Molecular Analysis of 3 Cases and a Survey of NUT Expression in Salivary Gland Carcinomas. *The American Journal of Surgical Pathology* 2018;**42**:877–84. doi:10.1097/PAS.0000000000001046.

34 Giridhar P, Mallick S, Kashyap L, Rath GK. Patterns of care and impact of prognostic factors in the outcome of NUT midline carcinoma: a systematic review and individual patient data analysis of 119 cases. *Eur Arch Otorhinolaryngol* 2018;**275**:815–21. doi:10.1007/s00405-018-4882-y.

35 French CA, Rahman S, Walsh EM, Kuhnle S, Grayson AR, Lemieux ME, Grunfeld N, Rubin BP, Antonescu CR, Zhang S, et al. NSD3-NUT Fusion Oncoprotein in NUT Midline Carcinoma: Implications for

a Novel Oncogenic Mechanism. *Cancer Discovery* 2014;**4**:928–41. doi:10.1158/2159-8290.CD-14-0014.

36 Agaimy A, Mueller SK, Bumm K, Iro H, Moskalev EA, Hartmann A, Stoehr R, Haller F. Intraductal Papillary Mucinous Neoplasms of Minor Salivary Glands With AKT1 p.Glu17Lys Mutation. *The American Journal of Surgical Pathology* 2018;**42**:1076–82. doi:10.1097/PAS.0000000000001080.

37 Rooper LM, Argyris PP, Thompson LDR, Gagan J, Westra WH, Jordan RC, Koutlas IG, Bishop JA. Salivary Mucinous Adenocarcinoma Is a Histologically Diverse Single Entity With Recurrent AKT1 E17K Mutations: Clinicopathologic and Molecular Characterization With Proposal for a Unified Classification. *Am J Surg Pathol* 2021. doi:10.1097/PAS.0000000000001688.

38 Lee Y-H, Huang W-C, Hsieh M-S. CTNNB1 mutations in basal cell adenoma of the salivary gland. *Journal of the Formosan Medical Association* 2018;**117**:894–901. doi:10.1016/j.jfma.2017.11.011.

39 Jo VY, Sholl LM, Krane JF. Distinctive Patterns of CTNNB1 (β-Catenin) Alterations in Salivary Gland Basal Cell Adenoma and Basal Cell Adenocarcinoma. *The American Journal of Surgical Pathology* 2016;**40**:1143–50. doi:10.1097/PAS.0000000000000669.

40 Sweeney RT, McClary AC, Myers BR, Biscocho J, Neahring L, Kwei KA, Qu K, Gong X, Ng T, Jones CD, et al. Identification of recurrent SMO and BRAF mutations in ameloblastomas. *Nat Genet* 2014;**46**:722–5. doi:10.1038/ng.2986.

41 Coura BP, Bernardes VF, de Sousa SF, França JA, Pereira NB, Pontes HAR, Batista AC, da Cruz Perez DE, de Albuquerque RLC Junior, de Souza LB, et al. KRAS mutations drive adenomatoid odontogenic tumor and are independent of clinicopathological features. *Modern Pathology* 2019;**32**:799–806. doi:10.1038/s41379-018-0194-4.

42 Morita M, Murase T, Okumura Y, Ueda K, Sakamoto Y, Masaki A, Kawakita D, Tada Y, Nibu K-I, Shibuya Y, et al. Clinicopathological significance of EGFR pathway gene mutations and CRTC1/3–MAML2 fusions in salivary gland mucoepidermoid carcinoma. *Histopathology* 2020;**76**:1013–22. doi:10.1111/his.14100.

43 Sebastiao APM, Xu B, Lozada JR, Pareja F, Geyer FC, Da Cruz Paula A, da Silva EM, Ghossein RA, Weinreb I, de Noronha L, et al. Histologic spectrum of polymorphous adenocarcinoma of the salivary gland harbor genetic alterations affecting PRKD genes. *Modern Pathology* 2020;**33**:65–73. doi:10.1038/s41379-019-0351-4.

44 Hsieh M-S, Bishop JA, Wang Y-P, Poh CF, Cheng Y-SL, Lee Y-H, Jin Y-T, Chang JYF. Salivary Sialadenoma Papilliferum Consists of Two Morphologically, Immunophenotypically, and Genetically Distinct Subtypes. *Head Neck Pathol* 2019;**14**:489–96. doi:10.1007/s12105-019-01068-4.

45 Weinreb I, Bishop JA, Chiosea SI, Seethala RR, Perez-Ordonez B, Zhang L, Sung Y-S, Chen C-L, Assaad A, Oliai BR, et al. Recurrent RET Gene Rearrangements in Intraductal Carcinomas of Salivary Gland. *Am J Surg Pathol* 2018;**42**:442–52. doi:10.1097/PAS.0000000000000952.

46 Luk PP, Weston JD, Yu B, Selinger CI, Ekmejian R, Eviston TJ, Lum T, Gao K, Boyer M, O'Toole SA, et al. Salivary duct carcinoma: Clinicopathologic features, morphologic spectrum, and somatic mutations. *Head & Neck* 2016;**38**:E1838–47. doi:10.1002/hed.24332.

47 Nakaguro M, Urano M, Ogawa I, Hirai H, Yamamoto Y, Yamaguchi H, Tanigawa M, Matsubayashi J, Hirano H, Shibahara J, et al. Histopathological evaluation of minor salivary gland papillary-cystic tumours: focus on genetic alterations in sialadenoma papilliferum and intraductal papillary mucinous neoplasm. *Histopathology* 2020;**76**:411–22. doi:10.1111/his.13990.

48 Kim Y, Song S, Lee M, Swatloski T, Kang JH, Ko Y-H, Park W-Y, Jeong H-S, Park K. Integrative genomic analysis of salivary duct carcinoma. *Sci Rep* 2020. doi:10.1038/s41598-020-72096-2.

49 Bishop JA, Gagan J, Baumhoer D, McLean-Holden AL, Oliai BR, Couce M, Thompson LDR. Sclerosing Polycystic "Adenosis" of Salivary Glands: A Neoplasm Characterized by PI3K Pathway Alterations More Correctly Named Sclerosing Polycystic Adenoma. *Head Neck Pathol* 2019;**14**:630–6. doi:10.1007/s12105-019-01088-0.

50 Haller F, Skálová A, Ihrler S, Märkl B, Bieg M, Moskalev EA, Erber R, Blank S, Winkelmann C, Hebele S, et al. Nuclear NR4A3 Immunostaining Is a Specific and Sensitive Novel Marker for Acinic Cell Carcinoma of the Salivary Glands. *The American Journal of Surgical Pathology* 2019;**43**:1264–72. doi:10.1097/PAS.0000000000001279.

51 Rechsteiner M, von Teichman A, Rüschoff JH, Fankhauser N, Pestalozzi B, Schraml P, Weber A, Wild P, Zimmermann D, Moch H. KRAS, BRAF, and TP53 Deep Sequencing for Colorectal Carcinoma Patient Diagnostics. *The Journal of Molecular Diagnostics* 2013;**15**:299–311. doi:10.1016/j.jmoldx.2013.02.001.

52 Rupp NJ, Rechsteiner M, Freiberger SN, Lenggenhager D, Urosevic M, Burger IA, Rushing EJ, Mihic-Probst D. New observations in tumor cell plasticity: mutational profiling in a case of metastatic melanoma with biphasic sarcomatoid transdifferentiation. *Virchows Arch* 2018;**473**:517–21. doi:10.1007/s00428-018-2376-3.

53 Rupp NJ, Brada M, Skálová A, Bode B, Broglie MA, Morand GB, Rechsteiner M, Freiberger SN. New Insights into Tumor Heterogeneity: A Case of Solid-Oncocytic Epithelial-Myoepithelial Carcinoma of the Parotid Gland Harboring a HRAS and Heterogeneous Terminating ARID1A Mutation. *Head Neck Pathol* 2019. doi:10.1007/s12105-019-01055-9.

54 Wang W, Xu C, Lei L, Wang X, Zhu Y, Fang Y, Cai X, Lin R, Lin L, Wang H, et al. Abstract 38: Large-scale study of NTRK fusions in Chinese solid tumors and using next generation sequencing: A multicenter study. *Cancer Res* 2020;**80**:38. doi:10.1158/1538-7445.AM2020-38.

55 Michal M, Kacerovska D, Kazakov DV. Cribriform Adenocarcinoma of the Tongue and Minor Salivary Glands: A Review. *Head Neck Pathol* 2013;**7**:3–11. doi:10.1007/s12105-013-0457-9.

56 Doebele RC, Drilon A, Paz-Ares L, Siena S, Shaw AT, Farago AF, Blakely CM, Seto T, Cho BC, Tosi D, et al. Entrectinib in patients with advanced or metastatic NTRK fusion-positive solid tumours: integrated analysis of three phase 1–2 trials. *Lancet Oncol* 2020;**21**:271–82. doi:10.1016/S1470-2045(19)30691-6.

57 Drilon A, Laetsch TW, Kummar S, DuBois SG, Lassen UN, Demetri GD, Nathenson M, Doebele RC, Farago AF, Pappo AS, et al. Efficacy of Larotrectinib in TRK Fusion–Positive Cancers in Adults and Children. *N Engl J Med* 2018;**378**:731–9. doi:10.1056/NEJMoa1714448.

58 Marchiò C, Scaltriti M, Ladanyi M, Iafrate AJ, Bibeau F, Dietel M, Hechtman JF, Troiani T, López-Rios F, Douillard J-Y, et al. ESMO recommendations on the standard methods to detect NTRK fusions in daily practice and clinical research. *Annals of Oncology* 2019;**30**:1417–27. doi:10.1093/annonc/mdz204.

59 Nguyen L, Chopra S, Laskar DB, Rao J, Lieu D, Chung F, Kim ED, de Peralta-Venturina M, Bose S, Balzer B. NOR-1 distinguishes acinic cell carcinoma from its mimics on fine-needle aspiration biopsy specimens. *Human Pathology* 2020;**102**:1–6. doi:10.1016/j.humpath.2020.05.001.

60 Skálová A, Agaimy A, Stanowska O, Baneckova M, Ptáková N, Ardighieri L, Nicolai P, Lombardi D, Durzynska M, Corcione L, et al. Molecular Profiling of Salivary Oncocytic Mucoepidermoid Carcinomas Helps to Resolve Differential Diagnostic Dilemma With Low-grade Oncocytic Lesions. *Am J Surg Pathol* 2020;**44**:1612–22. doi:10.1097/PAS.0000000000001590.

61 Todorovic E, Dickson BC, Weinreb I. Salivary Gland Cancer in the Era of Routine Next-Generation Sequencing. *Head and Neck Pathol* 2020;**14**:311–20. doi:10.1007/s12105-020-01140-4.

62 Weinreb I, Seethala RR, Perez-Ordoñez B, Chetty R, Hoschar AP, Hunt JL. Oncocytic Mucoepidermoid Carcinoma: Clinicopathologic Description in a Series of 12 Cases. *The American Journal of Surgical Pathology* 2009;**33**:409–16. doi:10.1097/PAS.0b013e318184b36d.

63 Seethala RR. An Update on Grading of Salivary Gland Carcinomas. *Head Neck Pathol* 2009;**3**:69–77. doi:10.1007/s12105-009-0102-9.

64 Makarenkova HP, Dartt DA. Myoepithelial Cells: Their Origin and Function in Lacrimal Gland Morphogenesis, Homeostasis, and Repair. *Curr Mol Biol Rep* 2015;**1**:115–23.

65 Bastaki JM, Purgina BM, Dacic S, Seethala RR. Secretory Myoepithelial Carcinoma: A Histologic and Molecular Survey and a Proposed Nomenclature for Mucin Producing Signet Ring Tumors. *Head Neck Pathol* 2014;**8**:250–60. doi:10.1007/s12105-014-0518-8.

66 El-Naggar A, Chan J, Grandis J, Takata T. *Slootweg P WHO Classification of Head and Neck Tumours*. 4th Edition. Lyon: IARC; 2017.

67 Ohtomo R, Mori T, Shibata S, Tsuta K, Maeshima AM, Akazawa C, Watabe Y, Honda K, Yamada T, Yoshimoto S, et al. SOX10 is a novel marker of acinus

and intercalated duct differentiation in salivary gland tumors: a clue to the histogenesis for tumor diagnosis. *Modern Pathology* 2013;**26**:1041–50. doi:10.1038/modpathol.2013.54.

68 Vander Poorten V, Triantafyllou A, Skálová A, Stenman G, Bishop JA, Hauben E, Hunt JL, Hellquist H, Feys S, De Bree R, et al. Polymorphous adenocarcinoma of the salivary glands: reappraisal and update. *Eur Arch Otorhinolaryngol* 2018;**275**:1681–95. doi:10.1007/s00405-018-4985-5.

69 Andreasen S, von Holstein SL, Homøe P, Heegaard S. Recurrent rearrangements of the PLAG1 and HMGA2 genes in lacrimal gland pleomorphic adenoma and carcinoma ex pleomorphic adenoma. *Acta Ophthalmologica* 2018;**96**:e768–71. doi:10.1111/aos.13667.

70 Katabi N, Ghossein R, Ho A, Dogan S, Zhang L, Sung Y-S, Antonescu CR. Consistent PLAG1 and HMGA2 abnormalities distinguish carcinoma ex-pleomorphic adenoma from its de novo counterparts. *Hum Pathol* 2015;**46**:26–33. doi:10.1016/j.humpath.2014.08.017.

71 Chênevert J, Duvvuri U, Chiosea S, Dacic S, Cieply K, Kim J, Shiwarski D, Seethala RR. DOG1: a novel marker of salivary acinar and intercalated duct differentiation. *Modern Pathology* 2012;**25**:919–29. doi:10.1038/modpathol.2012.57.

72 Leivo I. Sinonasal Adenocarcinoma: Update on Classification, Immunophenotype and Molecular Features. *Head and Neck Pathol* 2016;**10**:68–74. doi:10.1007/s12105-016-0694-9.

73 Rooper LM, Thompson LDR, Gagan J, Oliai BR, Weinreb I, Bishop JA. Salivary Intraductal Carcinoma Arising within Intraparotid Lymph Node: A Report of 4 Cases with Identification of a Novel STRN-ALK Fusion. *Head and Neck Pathol* 2020. doi:10.1007/s12105-020-01198-0.